An Interconnectivity Index for Osteoporosis Assessment Using X-Ray Images

Khaled Harrar[1,2,*] Latifa Hamami[1]

[1]Laboratoire Signal et Communications, Département d'Electronique, Ecole Nationale Polytechnique, 16200 Alger, Algérie
[2]Département Maintenance Industrielle, Faculté des Sciences de l'Ingénieur, Université M'Hamed Bougara Boumerdes, 35000 Boumerdes, Algérie

Received 6 Sep 2012; Accepted 29 Nov 2012; doi: 10.5405/jmbe.1294

Abstract

Osteoporosis is a condition that is characterized by low bone mass and microarchitectural deterioration of bone tissue, leading to enhanced bone fragility and a consequent increase in fracture risk. This paper develops an interconnectivity index for trabecular bone microarchitecture characterization for the discrimination of patients with different degrees of osteoporosis. A total of seventy one images of the calcaneus (heel bone) from subjects suffering from osteoporosis at different stages were analyzed. A fractal-based method (lacunarity), which quantifies the porosity of the bone, is used as a comparative tool to estimate correlations between interconnectivity indexes and the disease. Bone features are used to classify the subjects using a support vector machine (SVM) classifier. The correlation between the proposed interconnectivity index and the disease was found to better than that between an existing index and the disease. Statistical analysis results suggest that the proposed parameter is efficient for monitoring bone strength and predicting future fracture risk. Moreover, results obtained using SVM with features from the proposed index provide better accuracy and smaller error for classifying patients compared to those obtained with an existing index.

Keywords: Osteoporosis, Texture analysis, Lacunarity, Interconnectivity index, Bone mineral density (BMD), Support vector machine (SVM)

1. Introduction

Osteoporosis is a skeletal disease characterized by low bone mass and deterioration of bone microarchitecture, leading to increased risk of fracture. [1]. Bone microarchitecture is an important factor to be taken into account in assessing bone strength, and is a complementary risk factor to bone mineral density (BMD) measurement [2]. Trabecular microarchitecture characterization cannot be routinely obtained by noninvasive methods and requires a bone biopsy with histomorphometric analysis. For this reason, researchers have developed noninvasive methods for characterizing trabecular bone microarchitecture [3,4].

One of the most used methods for characterizing trabecular bone is that based on fractals. Fractal models are suited for describing medical image textures, with fractal dimension often used as a descriptor in texture analysis [5-7]. Lacunarity, which is another descriptor of texture, was introduced for measuring the distribution of voids in a geometric object, with the object being more lacunar than others if its void sizes are distributed over a wider range [8]. This property plays an important role in the study of the microarchitecture of trabecular bone. Osteoporotic stages are related to bone porosity, i.e, the more the bone is porous, the higher the severity of the disease.

There are other methods for assessing bone architecture. In particular, histomorphometry is a quantitative study of the organization of trabeculae of a bone tissue. Through the process of skeletonization of the trabecular bone image, it is possible to obtain the so called interconnectivity index, which is the connectivity of the marrow cavities or bone trabecular network.

A lot of work has been done to characterize the trabecular architecture. Marwan *et al*. [9] used fractal properties and spatial auto-correlation. The measure of lacunarity complexity, Moran's I index, and Geary's C index were defined for the three-dimensional image analysis of trabecular bone. The main finding is that the trabecular structure complexity decreases during bone loss. Nishihara *et al*. [10] developed an algorithm that can distinguish the central part of the vertebral body from abdominal X-ray computed tomography images to determine whether it is possible to aid the diagnosis of osteoporosis. Rachidi *et al*. [11] applied Laws' masks descriptors to bone texture analysis. Their study showed the dependence of Laws' masks parameters on image resolution, which confirms the necessity to perform Laws' textural measurement on high-resolution images.

* Corresponding author: Khaled Harrar
Tel: +213-0-550446659; Fax: +213-0-21522973
E-mail: harrar_k@umbb.dz

The present study develops and validates the new interconnectivity index (*NDX*), which is more effective than an existing interconnectivity index (*ICI*) in terms of the ability to discriminate patients with different degrees of osteoporosis. The limitation of *ICI* is that it does not consider all architectural parameters of the bone. Some connectivity and disruption parameters are neglected even though they provide information on the stiffness of the trabecular bone network. The proposed interconnectivity index takes into account new architectural parameters to provide better discrimination of subjects. In this study, a method based on fractal analysis (lacunarity) was used to find correlations between the two indexes and lacunarity. The best correlation was found between the proposed interconnectivity index and lacunarity. The proposed index provides the best performance in terms of discriminating subjects.

A support vector machine (SVM) classifier was used to compare the performance of *ICI* and *NDX* in terms of ability to discriminate between subjects. Two SVM classifiers are compared, namely those that include parameters used in *ICI* and *NDX*, respectively, to highlight the proposed parameters. The results show good performance in classification of subjects using the proposed index.

2. Materials and methods

2.1 Subjects and image acquisition

This study involved 71 women divided into four groups according to BMD measurements: 11 normal subjects (NO), aged 58 ± 6.34 years, 19 subjects with onset of osteoporosis (OP) (with physiological loss of calcium), aged 64 ± 7.80 years, 31 osteoporotic subjects (OS) (with abnormal loss of calcium), aged 70 ± 8.02 years, and 10 severe osteoporotic subjects (SOS) (with a risk of fracture), aged 79 ± 10.55 years.

Radiographic images of the calcaneus were taken following a standardized procedure obtained on a Kodak Min R screen-film system. The calcaneus was used because of the limited soft tissues surrounding this bone. Soft tissues could increase variability. The study of the calcaneus is relevant because it contains 90% trabecular bone [12] and is a good predictive site of fracture in terms of BMD [12]. The same radiographic parameters were used for all subjects. The focal distance was set at 1.15 m. The X-ray parameters were 55 kV and 20 mAs for all patients. Scanning the heel permitted the selection of a similar measurement site (region of interest (ROI)) for each subject by using anatomical landmarks, as previously described [12]. These anatomical landmarks were localized by the operator on the image, allowing positioning of the ROI (1.6 × 1.6 cm^2). The ROI was digitized with a CCD camera to a format with 256 × 256 pixels in gray scale (Fig. 1).

2.2 Image preprocessing

ROI images were first converted to binary using the algorithm described by White and Rudolph [13], which was used for measuring the morphologic features of the trabecular architecture. Each ROI image was first smoothed using a low-pass Gaussian filter (sigma = 21 pixels, kernel size = 10) to remove large-scale variations in the image. The smoothed image was then subtracted from the original, and a 128-gray-level value was added to each pixel of the subtracted image. The resulting image was then binarized using a global threshold value of 128 (Fig. 2) [13], which segmented the image into the bone (gray level of 255) and marrow (gray level of 0).

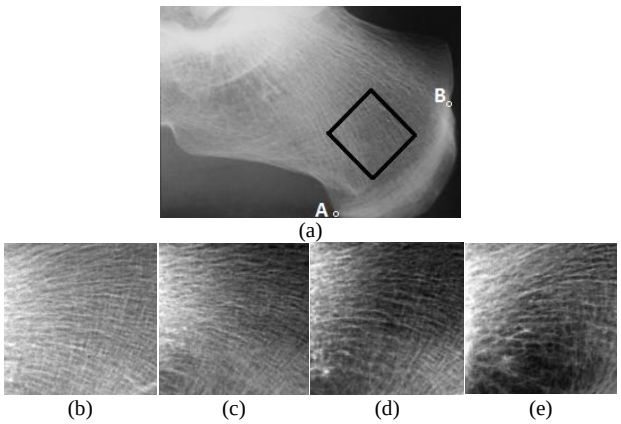

Figure 1. (a) ROI in lateral radiograph of the calcaneus with anatomical landmarks A and B. Texture images for (b) a normal case, (c) an osteopenic patient, (d) an osteoporotic patient, and (e) a severe osteoporotic case.

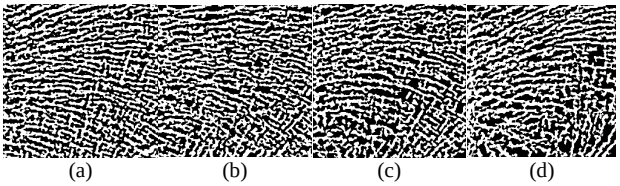

Figure 2. Binary images related to the previous ROI. (a) Control case, (b) osteopenic patient, (c) osteoporotic patient, and (d) severe osteoporotic case.

2.3 Lacunarity: gliding-box algorithm

In geometry, lacunarity (Λ) is a measure of how a fractal fills space. Lacuna means gap (more gaps = higher lacunarity). Various methods for calculating lacunarity have been proposed [14-16]. The gliding-box algorithm exhaustively samples an image using overlapping square windows of length *r*. It is based on a localized mass calculation [7,15]; a unit box of size *r* is chosen and the number of set points, *p*, within it (the mass) is counted. This procedure is then repeated, creating a distribution of box masses *D(p, r)*, where *D* is the number of boxes with *p* points and radius *r*. This distribution is converted into a probability distribution, *Q(p, r)*, by dividing *D(p, r)* by the total number of boxes *N(r)* of size *r*. The lacunarity at scale *r* is defined by the mean-square deviation of the fluctuation of mass distribution probability *Q(p, r)* divided by its square mean. Gliding-box lacunarity is then defined as:

$$\Lambda_{BG}(r) = \frac{Z^{(2)}(r)}{Z^{(1)}(r)^2} = \frac{\sum_p p^2 Q(p,r)}{[\sum_p pQ(p,r)]^2} \quad (1)$$

An extended version of lacunarity and the gliding-box concept was introduced by Plotnick *et al*. [17] based on a

random binary map (0 for empty and 1 for occupied):

$$\Lambda(r) = 1 + \frac{\sigma^2(r)}{\mu^2(r)} \quad (2)$$

where μ is the mean and σ^2 is the variance of the number of occupied sites at scale r. Lacunarity can be compared independently of image density by normalizing Eq. (2) [14]:

$$\Lambda_{norm} = 2 - \left(\frac{1}{\Lambda} + \frac{1}{\Lambda^c}\right) \quad (3)$$

where Λ^c is complementary lacunarity (obtained by calculating the lacunarity of the complement binary image). Λ_{norm} is denoted below as Λ for convenience.

2.4 Characterization of trabecular network

Several histomorphometric methods have been proposed to characterize the trabecular network. Some of them can screen diseases related to bone fragility at an early stage [18,19]. Topological characterization provides a quantification of loss in the connectivity of the tissue. It consists of counting trabecular plates and marrow spaces, as well as nodes connecting the plates. Skeletonization involves simplifying a binary image by reducing apparent trabecular thickness to the minimum value of 1 pixel [20]. The skeletonized image can be used to identify the connectivity parameters.

2.4.1. Connectivity parameters

The connectivity parameters are calculated from the characteristics of the skeletonized image of the trabecular structure. These parameters are obtained from trabecular profiles and the count of their connections in two-dimensional sections is obtained using a computed analysis called strut analysis (Fig. 3).

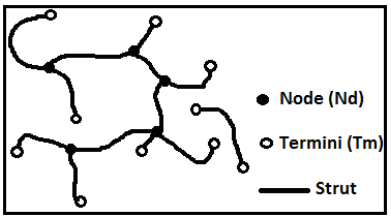

Figure 3. Strut analysis. Measurements of trabecular profiles and their connections on two-dimensional sections.

The trabecular network, defined as connectivity, is a three-dimensional property that describes the topology of the various connections between the nodes and the connecting segments (struts and termini). The struts refer to trabeculae. A link between three or more struts constitutes a node. When one side of a strut is not joined to a node, it is referred to as a free end or termini, which represents an interruption in the trabecular network [21].

2.4.2. New interconnectivity index (NDX)

2.4.2.1. Interconnectivity index (ICI)

The existing *ICI* was originally proposed by Le *et al*. [22] to describe the connectivity of porous biomaterials. It is based on the inverse architectural relationships between the trabecular network and marrow spaces: the more the trabecular network is disconnected, the more the marrow spaces will be connected. The total number of nodes (*Nd*), the number of node-to-node branches (*NNd*), and the number of node-to-termini branches (*NNdTm*) are determined, where a branch refers to a strut. Also, the number of trees (*T*) is obtained, where a tree is a structure composed of interconnected nodes with node-to-node and/or node-to-termini branches.

The *ICI* of bone-marrow cavities is defined as follows [23]:

$$ICI = \frac{Nd \times NNd}{T \times (NNdTm + 1)} \quad (4)$$

The higher the interconnectivity of the marrow (characterized by high numbers of nodes and segmental branches and few trees), the higher the *ICI* and the fragmentation of the trabecular network [22].

Since the purpose of the present study is to quantify loss of bone mass, the connectivity of the trabecular bone rather than that of the marrow cavities is considered. The interconnectivity index of the marrow was thus changed to that of the trabecular bone. In this case, the higher the connectivity of the trabecular network, the higher the index (*ICI*).

The existing interconnectivity index does not consider all the architectural parameters of bone structure. Some connectivity and disruption parameters are neglected even though they can provide more information on the stiffness of the trabecular network structure. The present study improves on *ICI* by developing the *NDX*, which takes into account such parameters.

2.4.2.2. Histological parameters

The study of microarchitecture is based on the measure of the width, number, and separation of trabeculae as well as on their spatial organization. These parameters describe the basic relationship between space and the trabecular network. Tissue volume (*TV*), bone surface (*BS*), and bone volume (*BV*) can be measured. In two-dimensional X-ray images, *TV* refers to the size of the image, *BS* is the perimeter of the bone, and *BV* is the area of the bone. The following parameters are determined [23]:

$$\text{Bone volume fraction: } V = \frac{BV}{TV} \times 100 \quad (5)$$

$$\text{Bone surface fraction: } S = \frac{BS}{TV} \times 100 \quad (6)$$

$$\text{Trabecular thickness: } TbTh = \frac{2}{BS / BV} \quad (7)$$

$$\text{Trabecular number: } TbN = \frac{BV / TV}{TbTh} \quad (8)$$

$$\text{Trabecular separation: } TbSp = \frac{1}{TbN} - TbTh \quad (9)$$

2.4.2.3. Topological parameters

To provide better characterization of the bone trabecular network to discriminate subjects, the following attributes are introduced:

Node-to-termini ratio: $R = Nd / Tm$ (10)

The node-to-termini ratio provides information about the rate of nodes relative to termini; this attribute is a connectivity parameter.

Number of branches whose ends are termini: *NTm*

This important parameter provides information about loss of connectivity in the bone architecture; this attribute is a disruption parameter.

Mean size of branches : $Dist = \frac{\sum br\_size}{NNdTm + NNd + NTm}$ (11)

where *br_size* is the size of the branches (whose ends are termini to termini, node to node, or node to termini).

The mean size of branches parameter (*Dist*) in topology analysis of the bone trabecular network is an important parameter that provides information on stiffness of the bone. Pathological patients have fewer branches than do healthy people, so their mean size of branches (*Dist*) is higher.

Taking into account these parameters, the *NDX* is defined as:

$$NDX = \frac{R \times NNd \times V \times TbTh}{(NTm + NNdTm) \times Dist \times TbSp} \quad (12)$$

The index combines all the parameters (histological and topological) to take advantage of the specific information provided by each. Some parameters favor connectivity (*R*, *NNd*, *V*, and *TbTh*), whereas others favor disruption (*NTm*, *NNdTm*, *Dist*, and *TbSp*). To get a high index corresponding to a strong bone for a healthy subject, the connectivity parameters should be in the numerator (with high values), and the disruption parameters should be in the denominator (which are low). For a pathological patient, the index should be low. High disruption and low connectivity parameters should be expected.

2.5 Patient classification and validation

This study used an SVM [24] classifier to classify subjects. SVM is a type of learning algorithm based on statistical learning theory, and is based on finding an optimal hyperplane for discriminating two classes.

Consider a training set $S = \{(x_i, y_i)\}_{i=1,..,n}$, where $x_i \in \Re^p$ is the attribute vector and $y_i \in \{1, -1\}$ is the class. A linear SVM is a linear discriminator of the form $D(x) = sgn(w^T x + b)$, where sgn is a sign function, $w \in \Re^p$ are the weights, and $b \in \Re$ are the biases. The weights and the biases are estimated by solving the following problem [24]:

$$\begin{cases} \max\limits_{w,b,\alpha} \ \frac{1}{2}\|w\|^2 - \sum\limits_{i=1}^{n} \alpha_i \left(y_i \left(w^T x_i + b \right) - 1 \right) \\ with \ \ \alpha_i \geq 0 \\ \qquad w - \sum\limits_{i=1}^{n} \alpha_i y_i x_i = 0 \quad and \quad \sum\limits_{i=1}^{n} \alpha_i y_i = 0 \end{cases} \quad (13)$$

where α_i are the set of Lagrange multipliers.

Generally, the optimal hyperplane is nonlinear. In this case, a nonlinear kernel function *k* is applied to maximum-margin hyperplanes. The transformation is nonlinear and the transformed space is high dimensional. The decision function becomes $D(x) = sgn(f(x) + b)$, with $f(x)$ given as [24]:

$$f(x) = \sum_{i=1}^{n} \alpha_i y_i k(x_i, x) \quad (14)$$

Generally, classification problems often use 2 classes (healthy and unhealthy), and are solved using binary methods. In this study, the discrimination of subjects is a multiclass [25] problem (4 classes). How can the 2-class problem be modified to solve a 4-class problem? Many classification systems have been developed for pattern classification problems using various algorithms, including SVM [26] and artificial neural networks [27]. Various methods allow extension from two-class problems to multiclass problems. For this, a multiclass problem is decomposed into multiple two-class classification problems.

In this study, the one-against all (OAA) method is used, in which each of the four classes is trained against all other classes. This approach has been recognized as an effective method [28]. The OAA approach is simple, powerful, and accurate [28]. To test and validate the classifier, the 10-fold cross-validation (CV) approach is used.

In this method, the dataset is divided into 10 folds. The classifier is trained with 9 folds and the last one is used for testing. This procedure is repeated for all folds (10 times); each time, one of them is selected as a test fold. The output of the classifier is estimated by averaging the accuracy obtained from each test set.

In this study the multiclass SVM classifier was used to classify the subjects and to compare the performance of *ICI* and *NDX*. Multiclass SVMs with input parameters used in *ICI* (*Nd, NNd, T, NNdTm*) and those used in *NDX* (*R, NNd, V, TbTh, NTm, NNdTm, Dist, TbSp*), respectively, were evaluated to highlight the proposed parameters.

3. Results

Linear correlation analysis was done using Pearson's r. The ability of the parameters to discriminate the four groups is given by the *p*-value obtained using the non-parametrical Kruskal-Wallis test (a test is considered as statistically significant if $p < 0.05$).

To evaluate the classification, the confusion matrix was used. The following properties were defined: standard error (*SE*), true positive (*TP*), false positive (*FP*) , true negative (*TN*), false negative (*FN*), true positive rate (*TPR* %), sensitivity, or recall = $TP/(TP + FN)$, false positive rate (*FPR* %) = (1 – specificity) = $FP/(FP + TN)$, specificity (*SPC*) or true negative rate = $TN/(TN + FP)$, positive predictive value (*PPV* %) or precision = $TP/(TP + FP)$, and accuracy (*Acc* %) = $(TP+TN)/(TP + FP + TN + FN)$.

The confusion matrix for a k-class classification problem is presented in Table 1, where C_i denotes the class label of the i^{th} class. From Table 1, for class *i*, the true positive $TP(i) = n_{ii}$

Table 1. Multiclass confusion matrix.

		Predicted class			
		C_1	C_2	……	C_k
True class	C_1	n_{11}	n_{12}	……	n_{1k}
	C_2	n_{21}	n_{22}	……	n_{2k}
	.	.	.	.	.
	.	.	.	.	.
	.	.	.	.	.
	C_k	n_{k1}	n_{k2}	……	n_{kk}

and the false positive $FP(i) = \sum_{j=1, j\neq i}^{k} n_{ji}$. The true negative, denoted by $TN(i)$, equals the sum of the elements of the confusion matrix with the column and row corresponding to class i removed, and the false negative, $FN(i) = \sum_{j=1, j\neq i}^{k} n_{ij}$. The classification accuracy is then defined as [26]:

$$Acc = \frac{\sum_{i=1}^{k} n_{ij}}{\sum_{i,j=1}^{k} n_{ij}} \tag{15}$$

In multiclass classification problems, accuracy is not suited for determining the classifier's performance on classifying each single class. The ability and the accuracy of recognizing relevant samples in multiclass classification are represented by the parameters *recall* (R_i) or *true positive rate* and *precision* (P_i). These parameters are defined as [26]:

$$R_i = \frac{n_{ii}}{\sum_{j=1}^{k} n_{ij}} \tag{16}$$

$$P_i = \frac{n_{ii}}{\sum_{j=1}^{k} n_{ji}} \tag{17}$$

All these properties were calculated for *ICI* and *NDX*, and were studied to evaluate classification performance.

The lacunarity scatter plots for the four subjects (binary test images) are shown in Fig. 4. The sampling boxes (r) are up to 25 pixels. The image of the patient suffering from osteoporosis with risk of fracture is the most lacunar. The image of the NO case has the lowest lacunarity.

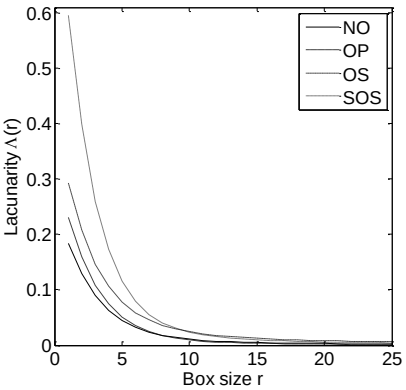

Figure 4. Lacunarity of the four cases in Fig. 1.

The classifications of the four groups obtained using *ICI* and *NDX* are given in Fig. 5. The new interconnectivity (*NDX*) provided better results in terms of discrimination of subjects (Fig. 5(b)). There is an overlap between groups for the existing interconnectivity index (Fig. 5(a)), suggesting that the proposed index is more reliable.

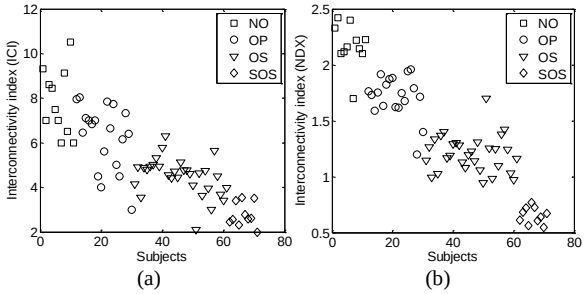

Figure 5. Classification of the four groups using (a) *ICI* and (b) *NDX*.

Figure 6 shows the interconnectivity indices (*ICI* and *NDX*) versus lacunarity for the 71 subjects. An inverse correlation between these two parameters is observed, with the coefficient of correlation between *NDX* and Λ (r = - 0.95, Fig. 6(b)) being higher than that between *ICI* and Λ (r = - 0.71, Fig. 6(a)).

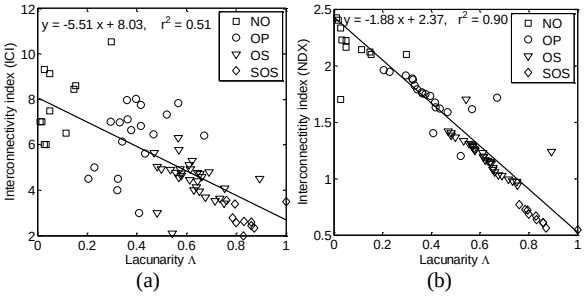

Figure 6. Interconnectivity index as function of lacunarity. Linear regressions of (a) *ICI* and (b) *NDX* versus Λ.

The coefficients of correlation between Λ, *ICI*, and *NDX* and all structural parameters are shown in Table 2. There is significant correlation between Λ, *ICI*, and *NDX*, and *BV*, *V*, *T*, *R*, and *NNd*. Furthermore, there is a weak correlation between Λ, *ICI*, and *NDX* and the other structural parameters. The best correlation was found between *NDX* and lacunarity. The new index gives the best results in terms of discrimination of subjects (p < 0.0001, Table 2).

The mean values of Λ, *ICI*, and *NDX* and the obtained standard deviations are presented in Fig. 7. The boxes represent

Table 2. Correlation between Λ, *ICI*, *NDX*, and structural parameters in 71 human radiographs.

Parameter	Λ	*ICI*	*NDX*	*p*-value
Λ	1	-0.71	-0.95	0.0003
ICI	-0.71	1	0.77	0.0007
NDX	-0.95	0.77	1	< 0.0001
BV	-0.81	0.72	0.85	0.001
BS	-0.02	-0.03	0.04	0.9
TV	Null	Null	Null	Ns*
TbN	0.02	-0.03	0.04	0.89
TbTh	-0.55	0.49	0.52	0.04
V	-0.81	0.72	0.85	0.001
S	0.55	-0.50	-0.52	0.04
TbSp	0.44	-0.37	-0.51	0.05
T	0.78	-0.74	-0.80	0.001
Nd	-0.64	0.48	0.67	0.003
Tm	0.39	-0.43	-0.39	0.02
R	-0.90	0.80	0.92	0.0004
NNd	-0.86	0.68	0.89	0.0009
NTm	0.71	-0.66	-0.73	0.73
NNdTm	0.16	-0.22	-0.14	0.004
Dist	0.47	-0.27	-0.50	0.0008

*Ns : Not significant

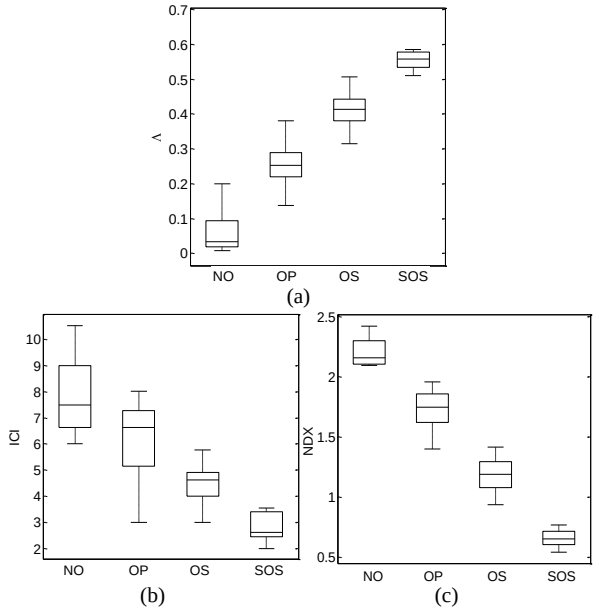

Figure 7. Mean ± SD values for (a) Λ, (b) ICI, and (c) NDX. The boxes represent 95% confidence intervals of the values.

95% confidence intervals of the values. Some overlap between the subjects can be observed for *Λ* and *ICI*, but not for *NDX*, for which a good separation is obtained. Tables 3 and 4 show confusion matrices for *ICI* and *NDX*, respectively. The SVM classifier using parameters used in *NDX* has high performance in terms of discrimination between subjects compared to that of the classifier using parameters used in *ICI*. The accuracy and rate of true detection were improved by introducing new architectural parameters.

Table 3. Confusion matrix of multiclass SVM using features included in *ICI* and validated by the 10-fold CV approach.

		Classified as						
		NO	OP	OS	SOS	*TPR*	*FPR*	Precision
Actual Classes	NO	5	6	0	0	45.5	6.7	55.6
	OP	4	9	5	1	47.4	17.3	50
	OS	0	3	26	2	83.9	20	76.5
	SOS	0	0	3	7	70	4.9	70
		ACC = 47/71 = 66.19 %						
		SE = 24/71 = 33.8 %						

Table 4. Confusion matrix of multiclass SVM using features included in *NDX* and validated by the 10-fold CV approach.

		Classified as						
		NO	OP	OS	SOS	*TPR*	*FPR*	Precision
Actual Classes	NO	10	1	0	0	90.9	0	90.9
	OP	0	17	2	0	89.5	3.8	89.5
	OS	0	1	30	0	96.8	5	96.8
	SOS	0	0	0	10	100	0	100
		ACC = 67/71 = 94.36 %						
		SE = 4/71 = 5.63 %						

4. Discussion

To monitor osteoporosis, hip and lumbar spine scans are used since these locations are considered as preferential measurement sites [29]. Measurements made at various sites show differences due to variability in the bone tissue [29]. The present study uses the calcaneus because of the limited soft tissues surrounding this bone. Soft tissues could increase the variability of the method. The study of the calcaneus seems relevant because it contains 90% of trabecular bone [12] and is a good predictive site of fracture in terms of BMD [12]. The proposed technique can be applied to any texture. Applying it to the spine or to the femoral neck should give satisfactory results. The only constraint is that the textures have to contain trabecular bone.

This work demonstrated a relationship between lacunarity and osteoporosis. Healthy subjects have low lacunarity values, whereas osteoporotic patients with risk of fracture have high lacunarity values (Fig. 4). Relationships between *ICI* and osteoporosis and between *NDX* and osteoporosis were demonstrated.

The interconnectivity indices (*ICI* and *NDX*) and connectivity parameters (*BV*, *TbN*, *TbTh*, *V*, *Nd*, R, *NNd*, *NNdTm*) are very high in control subjects and a young population due to strong connectivity of the trabecular bone. These parameters decrease in osteopenic cases due to early loss of connectivity. In osteoporotic patients, due to loss of bone mass and trabecular network connectivity, the trabeculae becomes very thin; and in severe osteoporotic cases, the subjects are at risk of fractures due to few trabeculae and nodes with increased number of free ends. Such a decrease in this index in osteoporosis patients reflects alterations of the trabecular bone microarchitecture linked to aging and menopause.

Lacunarity, which provides information about the porosity of the bone structure, is jointly linked to the interconnectivity indices (*ICI* and *NDX*). The more lacunarity increases, the more connectivity decreases. This could correspond to bone alterations due to architectural disorganization of the trabecular network, which agrees with the expected results (Figs. 6(a) and (b)). From simple regression analysis, the strongest correlation was found between *Λ* and *NDX* (Table 2). According to the r^2 value, 90% of the variability of the fractal lacunarity parameter was determined by the new interconnectivity index. The simple correlation between *NDX* and the new structural parameter *R* was also significant, with an r coefficient of 0.92. A significant correlation was found between *NDX* and some parameters (*ICI*, *BV, V, T, NNd, NTm*), but no correlation was found with other parameters (*BS, TV, TbN, Tm, NNdTm*) (Table 2). These correlations reflect the fact that there is a discrepancy between these parameters: a rigid bone structure may have more free ends than a fragile structure if it contains more nodes, trees, and branches. The limits of the existing index *ICI* are due to it not considering all architectural parameters of the bone structure. It neglects some connectivity and disruption parameters. The proposed index represents the combination of several parameters, providing more information on the stiffness of a bone structure. All these parameters together, rather than separately, better explain the variance of the *NDX* parameter. In terms of discrimination of subjects, there is variability in Table 2, but the best performance is obtained by the new interconnectivity index, which had the best ability to discriminate subjects ($p < 0.0001$). This index is more accurate and reliable than *ICI* since it has the highest coefficient of correlation ($r = -0.95$ for *NDX* versus $r = -0.71$ for *ICI*), with overlap between groups using *ICI* (Fig. 5(a)).

Comparing classification results using multiclass SVM with 10-fold CV, Tables 3 and 4 reveal that the proposed index has the best performance, with high precision and high rate of true prediction, whereas the results of classification obtained using parameters used in *ICI* were poor, with more false detection. Most previous studies used 2 groups of patients (healthy and osteoporotic). In contrast, the present study used all groups of patients defined by the World Health Organization (healthy, osteopenic, osteoporotic, and severe osteoporotic patients).

5. Conclusion

This study developed and validated a new interconnectivity index that takes into account new architectural parameters to discriminate subjects suffering from osteoporosis. The proposed index had a higher correlation coefficient value (r = -0.95) and a lower p-value ($p < 0.0001$) compared to those of an existing index. To highlight the use of new parameters, multiclass SVMs were used to classify subjects. The results show that the proposed index achieved 94.36% correct classification, whereas the existing index achieved just 66.19% correct classification. In conclusion, histomorphometry and fractal analysis of bone texture from calcaneus radiographs are considered as simple, low-radiation, and reproducible techniques for assessing bone fragility. Being independent of bone density, these methods could be complementary to BMD measurements. Several techniques (fractal analysis, structural methods) need to be used in parallel to understand the pathophysiological mechanisms of osteoporotic states.

Acknowledgment

The authors wish to thank Prof. R. Jennane for his help.

References

[1] J. M. Vogel, P. J. Manly and R. D. Wasnich, "Densitometer for scanning OS calcis for predicting osteoporosis," *Comput. Med. Imaging Graph.*, 14: XI-XII, 1990.

[2] E. Martín-Badosa, A. Elmoutaouakkil, S. Nuzzo, D. Amblard, L. Vico and F. Peyrin, "A method for the automatic characterization of bone architecture in 3D mice microtomographic images," *Comput. Med. Imaging Graph.*, 27: 447-458, 2003.

[3] P. Pulkkinen, T. Jämsä, E. M. Lochmüller, V. Kuhn, M. T. Nieminen and F. Eckstein, "Experimental hip fracture load can be predicted from plain radiography by combined analysis of trabecular bone structure and bone geometry," *Osteoporos. Int*., 19: 547-558, 2008.

[4] N. Dalzell, S. Kaptoge, N. Morris, A. Berthier, B. Koller, L. Braak, B. van Rietbergen and J. Reeve, "Bone micro-architecture and determinants of strength in the radius and tibia: age-related changes in a population-based study of normal adults measured with high-resolution pQCT," *Osteoporos. Int*., 20: 1683-1694, 2009.

[5] K. Harrar and L. Hamami, "Implementation of the box-counting method in radiographic images," in: N. Mastorakis and J. Sakellaris (Ed.), *Advances in Numerical Methods*, Springer Science Business Media, 299-311, 2009.

[6] K. Harrar and L. Hamami, "The Fractal Dimension correlated to the bone mineral density," *WSEAS Trans. Sign. Process*., 4: 110-126, 2008.

[7] B. B. Mandelbrot, *The Fractal Geometry of Nature*, Freeman. San Francisco: CA, 1983.

[8] R. A. Feagin, "Relationship of second-order lacunarity, Hurst exponent, Brownian motion, and pattern organization," *Physica A*, 328: 315-321, 2003.

[9] N. Marwan, P. Saparin and J. Kurths, "Measures of complexity for 3D image analysis of trabecular bone," *Eur. Phys. J.-Spec. Top*., 143: 109-116, 2007.

[10] S. Nishihara, H. Fujita, T. Iida, A. Takigawa, T. Hara and X. Zhou, "Evaluation of osteoporosis in X-ray CT examination: A preliminary study for an automatic recognition algorithm for the central part of a vertebral body using abdominal X-ray CT images," *Comput. Med. Imaging Graph.*, 29: 259-266, 2005.

[11] M. Rachidi, A. Marchadier, C. Gadois, E. Lespessailles, C. Chappard and C. L. Benhamou, "Laws' masks descriptors applied to bone texture analysis: an innovative and discriminant tool in osteoporosis," *Skeletal Radiol*., 37: 541-548, 2008.

[12] C. L. Benhamou, E. Lespessailles, G. Jacquet, R. Harba, R. Jennan, T. Loussot, D. Tourliere and W. Ohley, "Fractal organization of trabecular bone images on calcaneus radiographs," *J. Bone Miner. Res*., 9: 1909-1918, 1994.

[13] S. C. White and D. J. Rudolph, "Alterations of the trabecular pattern of the jaws in patients with osteoporosis," *Oral Surg. Oral Med. Oral Pathol. Oral Radiol. Endod*., 88: 628-635, 1999.

[14] G. Dougherty, "A comparison of the texture of computed tomography and projection radiography images of vertebral trabecular bone using fractal signature and lacunarity," *Med. Eng. Phys*., 23: 313-321, 2001.

[15] C. Allain and M. Cloitre, "Characterizing the lacunarity of random and deterministic fractal sets," *Phys. Rev. A*., 44: 3552-3558, 1991.

[16] R. Voss, "Random fractals: characterization and measurement," in: R. Pynn and A. Skjeltorp (Ed.), *Scaling phenomena in disordered systems*, New York: Plenum, 1-11, 1985a.

[17] R. E. Plotnick, R. H. Gradner, W. W. Hargrove, K. Prestegaard and M. Perlmutter, "Lacunarity analysis: a general technique for the analysis of spatial patterns," *Phys. Rev. E Stat. Phys. Plasmas Fluids Relat. Interdiscip. Topics*, 53: 5461-5468, 1996.

[18] L. Dalle Carbonare, M. T. Valenti, F. Bertoldo, M. Zanatta, S. Zenari, G. Realdi, V. Lo Cascio and S. Giannini, "Bone microarchitecture evaluated by histomorphometry," *Micron*, 36: 609-616, 2005.

[19] R. R. Recker, D. B. Kimmel, D. Dempster, R. S. Weinstein, T. J. Wronski and D. B. Burr, "Issues in modern bone histomorphometry," *Bone*, 49: 955-964, 2011.

[20] N. J. Garraghan, R. W. E. Mellish and J. E. Compston, "A new method for two-dimensional analysis of bone structure in human iliac crest biopsies," *J. Microsc*., 142: 341-349, 1986.

[21] A. M. Parfitt, "Remodeling and microstructure of bone: Relation to prevent of age related fracture," in: A. Vagenakis, P. Soucacos, A. Avramides, G. Segre and L. Deftos (Ed.), *Second Int. Conf. Osteoporosis: Social and Clinical Aspects*, Italia Editori SIA, Milano: Masson, 197-209, 1986.

[22] H. M. Le, R. E. Holmes, E. C. Shors and D. A. Rosenstein, "Computerized quantitative analysis of the interconnectivity of porous biomaterials," *Acta Stereol*., 11: 267-272, 1992.

[23] D. Chappard, M. F. Baslé, E. Legrand and M. Audran, "Trabecular bone microarchitecture: A review," *Morphol. Bull. Assoc. Anat*., 92: 162-170, 2008.

[24] C. Cortes and V. N. Vapnik, "Support vector networks," *Mach. Learn*., 20: 273-297, 1995.

[25] M. R. Homaeinezhad, A. Ghaffari and R. Rahmani, "Review: Multi-lead discrete wavelet-based ECG arrhythmia recognition via sequential particle support vector machine classifiers," *J. Med. Biol. Eng*., 32: 381-396, 2012.

[26] C. Hsu and C. Lin, "A comparison of methods for multiclass support vector machines," *IEEE Trans. Neural Netw*., 13: 415-425, 2002.

[27] C. M. Bishop, *Neural Networks for Pattern Recognition*, Oxford University Press, Oxford, 1995.

[28] R. Rifkin and A. Klautau, "In defense of one-vs-all classification," *J. Mach. Learn. Res*., 5: 101-141, 2004.

[29] D. Marshall, O. Johnell and H. Wedel, "Meta-analysis of how well measures of bone mineral density predict occurrence of osteoporotic fractures," *Br. Med. J*., 312: 1254-1259, 1996.